Development of Fibrin Branch Structure Before and After Gelation
A.L. Fogelson, A.C. Nelson, C. Zapata-Allegro, J.P. Keener

S1. Supplement.

S1.1. Derivation of formulas for θ_s and B_s. The mass density of oligomers in the sol is $\theta_s(\mathbf{x},t) = \sum_{m,b}(m+2b)c_{mb}$. Recall that $g(\mathbf{x},t,y,z) = \sum_{m,b} y^m z^{b+2} c_{mb}$. By computing the appropriate derivatives of g, it is immediate that $\theta_s = (g_y + 2g_z - 4g)|_{y=z=1}$. From the definition of $\tilde{W}$, we have that $g_z = zR - \tilde{W}$. Integrating this from $z = 0$ to $z = 1$ and noting that $g(\mathbf{x},t,y,z=0) = 0$, we obtain

$$g(\mathbf{x},t,y,1) = \frac{R}{2} - \int_0^1 \tilde{W}(\mathbf{x},t,y,z')dz',$$

and from this it follows that $g_y(\mathbf{x},t,y,1) = -\int_0^1 \tilde{W}_y(\mathbf{x},t,y,z')dz'$. Recalling that $W_y(\mathbf{x},t,1,z) = V(\mathbf{x},t,z)$, this yields $g_y(\mathbf{x},t,1,1) = -\int_0^1 V(\mathbf{x},t,z')dz'$. Since also $W(\mathbf{x},t,z) = \tilde{W}(\mathbf{x},t,1,z)$, we have that

$$\theta_s(\mathbf{x},t) = -\int_0^1 V(\mathbf{x},t,z')dz' + (2R - 2W(\mathbf{x},t,1)) - 4\left(\frac{R}{2} - \int_0^1 W(\mathbf{x},t,z')dz'\right)$$

$$= 4\int_0^1 W(\mathbf{x},t,z')dz' - 2W(\mathbf{x},t,1) - \int_0^1 V(\mathbf{x},t,z')dz'.$$

The concentration of branches on soluble oligomers is $B_s(\mathbf{x},t) = \sum_{m,b} b c_{mb}$. This is the same as $B_s(\mathbf{x},t) = g_z(\mathbf{x},t,1,1) - 2g(\mathbf{x},t,1,1)$. Since $g_z(\mathbf{x},t,y,z) = zR(\mathbf{x},t) - \tilde{W}(\mathbf{x},t,y,z)$, we have $g_z(\mathbf{x},t,1,1) = R(\mathbf{x},t) - \tilde{W}(\mathbf{x},t,1,1) = R(\mathbf{x},t) - W(\mathbf{x},t,1)$. As noted above, $g(\mathbf{x},t,1,1) = \frac{R}{2} - \int_0^1 W(\mathbf{x},t,z')dz'$. Hence, $B_s(\mathbf{x},t) = 2\int_0^1 W(\mathbf{x},t,z')dz' - W(\mathbf{x},t,1)$.

S1.2. Diffusion of monomer. Suppose monomer diffuses with diffusion coefficient D_1. Then, the monomer concentration c_{10} evolves according to the equation

(S1.1) $$(c_{10})_t = \nabla \cdot (D_1 \nabla c_{10}) - 2k_l c_{10} R - k_b c_{10}(R^2 - R_g^2) + S_{10}.$$

Writing $\nabla \cdot (D_1 \nabla c_{10}) = \nabla \cdot (D \nabla c_{10}) + \nabla \cdot ((D_1 - D)\nabla c_{10})$, we find that the partial differential equation for g is modified by the addition of the term $\{\nabla \cdot ((D_1 - D)\nabla c_{10})\} y z^2$ on the right hand side, and that for R by the addition of the term $2\nabla \cdot ((D_1 - D)\nabla c_{10})$. Consequently, the equations for $\tilde{W} = zR - g_z$ and $\tilde{W}_y$ are modified, respectively, by the addition of terms $2z(1-y)\nabla \cdot ((D_1 - D)\nabla c_{10})$ and $-2z\nabla \cdot ((D_1 - D)\nabla c_{10})$. Hence, the equations for W, V, and R are modified, respectively, by the addition of terms 0, $-2z\nabla \cdot ((D_1 - D)\nabla c_{10})$, and $2\nabla \cdot ((D_1 - D)\nabla c_{10})$. Similarly, an additional term $\nabla \cdot ((D_1 - D)\nabla c_{10})$ appears on the right hand side of the equation for θ.

S1.3. Relation between R_g and B_g. We can write the equations for W and B in the form

$$W_t = \nabla \cdot (D\nabla(W - zR_g) - F_z + r^W,$$

$$B_t = \nabla \cdot (D\nabla B_s) + r^B,$$

where

$$F(z,\mathbf{x},t) = k_l \frac{W^2}{2} + k_b\left(\frac{1}{6}(zR - W)^3 - \frac{1}{2}(R^2 - R_g^2)z(zR - W)\right),$$

$$r^W(z,\mathbf{x},t) = k_l z R_g^2 - k_b \frac{z}{2}\left(R^3 - (3R_s R_g^2 + R_g^3)\right),$$

1

$$r^B(\mathbf{x}, t) = k_b \frac{1}{6}\left(R^3 - (3R_s R_g^2 + R_g^3) \right),$$

$$R_g(\mathbf{x}, t) = W(\mathbf{x}, t, 1), \qquad R_s(\mathbf{x}, t) = R - R_g,$$

$$B_s(\mathbf{x}, t) = 2 \int_0^1 W(\mathbf{x}, t, z') dz' - R_g, \qquad B_g(\mathbf{x}, t) = B - B_s.$$

Note that

$$B_g(\mathbf{x}, t) = B(\mathbf{x}, t) - 2 \int_0^1 W(\mathbf{x}, t, z') dz' + R_g(\mathbf{x}, t).$$

and that $B_g(\mathbf{x}, t) = R_g(\mathbf{x}, t) = 0$ for $t < t_{gel}^-$, so $B(\mathbf{x}, t) - 2 \int_0^1 W(\mathbf{x}, t, z') dz' = 0$ for all such t and for all $\mathbf{x}$. If $B(\mathbf{x}, t) - 2 \int_0^1 W(\mathbf{x}, t, z') dz' = 0$ for all $t \geq t_{gel}$, then $B_g(\mathbf{x}, t) = R_g(\mathbf{x}, t)$ for all t. So we consider,

$$\frac{\partial}{\partial t}\left(B(\mathbf{x}, t) - 2 \int_0^1 W(\mathbf{x}, t, z') dz' \right).$$

Using the equations above, we find that,

$$\frac{\partial}{\partial t} B(\mathbf{x}, t) = \nabla \cdot \left(D\nabla\left(2 \int_0^1 W(\mathbf{x}, t, z') dz' - R_g(\mathbf{x}, t) \right) \right) + r^B(\mathbf{x}, t),$$

and

$$\frac{\partial}{\partial t}\left(\int_0^1 W(\mathbf{x}, t, z') dz' \right) = -F(1, \mathbf{x}, t) + F(0, \mathbf{x}, t) + \int_0^1 r^W(\mathbf{x}, t, z') dz'$$

$$+ \nabla \cdot \left(D\nabla\left(\int_0^1 W(\mathbf{x}, t, z') dz' - \frac{1}{2} R_g(\mathbf{x}, t) \right) \right).$$

Using these last two equations and after some algebra,

$$\frac{\partial}{\partial t}\left(B(\mathbf{x}, t) - 2 \int_0^1 W(\mathbf{x}, t, z') dz' \right) = r^B(\mathbf{x}, t) + 2F(1, \mathbf{x}, t) - 2 \int_0^1 r^W(\mathbf{x}, t, z') dz' = 0,$$

and consequently $B_g(\mathbf{x}, t) \equiv R_g(\mathbf{x}, t)$.

S1.4. Boundary Conditions. We assume that c_{mb} satisfies the boundary conditions

(S1.2) $$- D\mathbf{n} \cdot \nabla c_{mb}(\mathbf{x}, t) = F_{10}(\mathbf{x}, t)\delta_{m1}\delta_{b0}.$$

Using these conditions and the definition of $g(\mathbf{x}, t, z, y)$, we see that

$$-D\mathbf{n} \cdot \nabla g(\mathbf{x}, t, y, z) = F_{10}(\mathbf{x}, t)yz^2 \quad \text{and} \quad -D\mathbf{n} \cdot \nabla g_z(\mathbf{x}, t, y, z) = 2F_{10}(\mathbf{x}, t)yz.$$

Recalling that $R_s(\mathbf{x}, t) = g_z(\mathbf{x}, t, 1, 1)$, we deduce that R_s satisfies the condition

(S1.3) $$- D\mathbf{n} \cdot \nabla R_s(\mathbf{x}, t) = 2F_{10}(\mathbf{x}, t),$$

which is consistent with the fact that each monomer has two reactive sites. Since $R = R_s + R_g$, it follows that

(S1.4) $$- D\mathbf{n} \cdot \nabla R(\mathbf{x}, t) = 2F_{10}(\mathbf{x}, t) - D\mathbf{n} \cdot \nabla R_g.$$

2

918 Because reactive sites on the gel do not move, the term $-D\nabla R_g$ should *not* be thought
919 of as the diffusive flux of gel reactive sites, but instead as the quantity needed to
920 account for the inclusion of R_g in R on the left-hand side of Eq. 2.34. Using the
921 definition $\tilde{W}(\mathbf{x}, t, y, z) = zR(\mathbf{x}, t) - g_z(\mathbf{x}, t, y, z)$, and the boundary conditions just
922 derived we find that

923
$$-D\mathbf{n} \cdot \nabla \tilde{W}(\mathbf{x}, t, y, z) = 2F_{10}(\mathbf{x}, t)z(1-y) - zD\mathbf{n} \cdot \nabla R_g(\mathbf{x}, t),$$
924
$$-D\mathbf{n} \cdot \nabla \tilde{W}_y(\mathbf{x}, t, y, z) = -2F_{10}(\mathbf{x}, t)z.$$

925 It follows that

926 (S1.5) $\quad -D\mathbf{n}\cdot\nabla W(\mathbf{x}, t, z) = -D\mathbf{n}\cdot\nabla R_g(\mathbf{x}, t) \ $ and $\ -D\mathbf{n}\cdot\nabla V(\mathbf{x}, t, z) = -2F_{10}(\mathbf{x}, t).$

927 Using Eqs. 2.27-2.28 and Eq. S1.5, we find that

928 (S1.6) $\qquad -D\mathbf{n} \cdot \nabla\theta_s(\mathbf{x}, t) = F_{10}(\mathbf{x}, t) \quad$ and $\quad -D\mathbf{n} \cdot \nabla B_s(\mathbf{x}, t) = 0.$

929   We note that the boundary conditions in Eqs. 2.36 hold automatically for θ_s and
930 B_s calculated from (2.27-2.28), but it is important to make explicit use of them in
931 discretizing the terms $D\Delta\theta_s$ and $D\Delta B_s$ in the PDEs 2.31 and 2.32, respectively. In
932 order to determine the monomer distribution c_{10}, we also solve the $m = 1$, $b = 0$
933 instance of Eqs. 2.18 and 2.33.

934   **S1.5. <u>Numerical solution of the PDEs.</u>** Consider our equations

935
$$W_t = D\big(W - zW|_{z=1}\big)_{xx}$$
936
$$- \left\{\frac{k_l}{2}W^2 + \frac{k_b}{6}\big(zR - W\big)^3 - \frac{k_b}{2}\big(R^2 - R_g^2\big)\big(z^2R - zW\big)\right\}_z$$
937
$$+ k_l z R_g^2 - \frac{k_b}{2}z\Big(R^3 - \big(3R_sR_g^2 + R_g^3\big)\Big).$$
938
$$R_t = D(R_s)_{xx} - k_l\,(R^2 - R_g^2)\, - \, \frac{k_b}{2}\,\Big(R^3 - \big(3R_sR_g^2 + R_g^3\big)\Big)\, + \, 2S_{10}.$$

939 Recalling that $R_g = W|_{z=1}$ and $R_s = R - R_g$, these equations have the form:

940
$$W_t = -(F(W, R))_z + D\big(W - zW|_{z=1}\big)_{xx} + r^W(W, R),$$
941
$$R_t = D(R_s)_{xx} + r^R(W, R).$$

942 To solve these equations numerically, we use a fractional step approach, first updating
943 W and R to account for transport in z and for the reactions terms $r^W(W, R)$ and
944 $r^R(W, R)$, and then updating them to account for diffusion in x. For the diffusion
945 term, we discretize in x using a uniform grid and the usual three-point approximation
946 to the second derivative within a Crank-Nicolson scheme. For the reaction terms
947 $r^W(W, R)$ and $r^R(W, R)$, we use an explicit two-stage Runge-Kutta scheme.
948   For the transport in z terms in the W PDE, we have to contend with the fact that
949 W_z develops a singularity at $z = 1$ at time $t = t_{gel}$, while it is smooth for $0 \le z < 1$
950 for all t, and the branch starting from $z = 0$ is smooth for $0 \le z \le 1$ for $t < t_{gel}$ and
951 $t > t_{gel}$. We do not have a boundary condition for W at $z = 1$. For these reasons,
952 we introduce a grid with much finer spacing close to $z = 1$, and for each point on this
953 grid, we use a blend of the upwind Beam-Warming (BW) scheme and the centered
954 Lax-Wendroff (LW) scheme. The blend is z-dependent, reducing to the BW scheme

3

close to $z = 1$ and to the LW scheme close to $z = 0$, where we do have a boundary condition for W.

For an equation $W_t = F(W)_z$, both the BW and LW schemes are based on the expansion

(S1.7) $$W(t + k, z) = W(t, z) - F(W)_z k + (((F'(W))^2 W_z)_z) k^2 / 2 + O(k^3).$$

For the BW scheme, we approximate $F(W)_z$ at z_j with a one-sided second order finite-difference quotient and we approximate $((Ff'(W))^2 W_z)_z)$ at z_j with the usual approximation to a variable-coefficient diffusion term, but evaluated at z_{j-1} rather than z_j. This introduces an $O(h)$ error for this quantity, but it is multiplied by k^2, and so the overall scheme is still second-order. For the LW scheme, we use a centered-difference approximation to $F(W)_z$ at z_j and the same approximation to the variable coefficient diffusion term as for BW but evaluated at z_j. More details about the numerical method can be found in [10].

S1.6. On the R_s steady-state assumption. We examine the origin of the gap in Fig, 10b, between the blue dashed line and the asymptotic limits of the colored curves as $k_b \to \infty$. According to the exact relationship Eq. 3.11, f^A is given by

(S1.8) $$f_A = \frac{2}{1 - \frac{B_s}{R_s}}.$$

In calculating the height of the dashed line, we use this formula but make the assumption that $R_s = r_{ss}$ is in steady-state, where r_{ss} satisfies Eq. 3.5 and we use an asymptotic value of r_{ss} to determine $B_s(t_{gel})$ using Eq. 3.9 for use in the Eq. 3.11. Fig. S1a shows the same colored curves as in Fig. 10b, as well as black dashed curves calculated from Eq. 3.11 using a numerical solution of Eq. 3.5. The black curves asymptote to the blue dashed line, so the use of the asymptotic value for r_{ss} is not the primary reason for the gap. In Fig. S1b we plot curves $R_s(t)$ vs t for a range of source rates S_{10} and branching rates k_b. Each curve ends at the time at which gelation occurs for the corresponding S_{10}, k_b pair. The ends of the curves are indicated by dots and the dot corresponding to the smallest value of k_b appears at the right end of each curve. For all source rates, S_{10}, steady state is attained by gel time for some of the smaller branching rate values. For $S_{10} = 10^{-5}$ steady state is attained for k_b between 10^{-5} and 10^1. For the $S_{10} = 10^5$, steady state is attained only for k_b between 10^{-5} and 10^{-3}. Furthermore, the gap between $R_s(t_{gel})$ and the steady-state value is large, in particular for large values of S_{10} and k_b.

S1.7. Showing that $f^A \to 3$. Our numerical evidence suggests that $f^A(t) = R(t)/M_{00}(t) \to 3$ as $t \to t_{gel}$ if only monomers are present initially and there is no additional source of monomers. Here, we show that this must be the case. The key equations are

(S1.9) $$\frac{dR}{dt} = -k_l R^2 - \frac{k_b}{2} R^3,$$

(S1.10) $$\frac{dY}{dt} = k_l Y^2 + k_b R \left(\frac{1}{2} R^2 + RY + Y^2 \right),$$

and

(S1.11) $$\frac{dM_{00}}{dt} = -\frac{k_l}{2} R^2 - \frac{k_b}{3} R^3$$
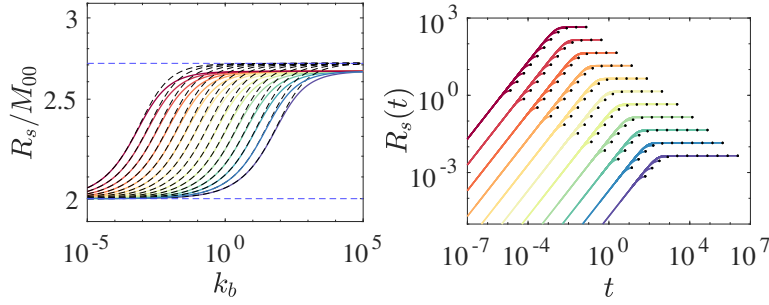
4

Fig. S1: ODE model simulations with constant source rate S_{10} increasing by factors of 10 from 10^{-5} (deep blue curve) to 10^5 (deep red curves) and branching rates k_b. (a) Average functionality $f^A = \frac{R_s}{M_{00}}$ at t_{gel}. Colored curves show results from numerical solutions of Eqs. 2.10-2.14. Dashed black curves show approximate f^A calculated from Eq. 3.11 using the numerical solution r_{ss} of Eq. 3.5. (b) Plots of $R_s(t)$ vs. t. k_b increases by factors of 10 from 10^{-5} to 10^5 with the right-most point of each curve corresponding to $k_b = 10^{-5}$.

Since we are interested in events before gel time, $R_s(t) = R(t)$. Eqs. S1.9 and S1.11 are the same as Eqs. 2.10 and 2.15 in the main text, respectively. The gelation indicator variable $U(t)$ in the main text is obtained from $Y(t)$ by a Riccati transformation $Y = -\frac{1}{aU}\frac{dU}{dt}$ where $a = k_l + k_b R$ [9]. The key point is that $U(t) \to 0$ if and only if $Y(t) \to \infty$, so the latter is also an indication of gelation. The relevant initial conditions are $R(0) = R_0$, $Y(0) = 0$, and $M_{00}(0) = \frac{R_0}{2}$.

Since Eq. S1.9 implies that $R(t)$ is a monotone decreasing of t, we can use R as the independent variable and from Eqs. S1.9-S1.11 we obtain

(S1.12)
$$\frac{dY}{dR} = -\frac{k_l Y^2 + k_b R\left(\frac{1}{2}R^2 + RY + Y^2\right)}{k_l R^2 + \frac{k_b}{2}R^3}$$

and

(S1.13)
$$\frac{dM_{00}}{dR} = \frac{\frac{k_l}{2}R^2 + \frac{k_b}{3}R^3}{k_l R^2 + \frac{k_b}{2}R^3}.$$

The solution of Eq. S1.12 is

(S1.14)
$$Y(R) = -R\frac{k_l \ln(k_b R + k_l) - \frac{k_b}{2}R + C}{k_l \ln(k_b R + k_l) - k_b R + C}.$$

Choosing the constant C so that $Y(R_0) = 0$ yields

(S1.15)
$$Y(R) = -R\frac{k_l \ln\left(\frac{k_b R + k_l}{k_b R_0 + k_l}\right) - \frac{k_b}{2}R + \frac{k_b}{2}R_0}{k_l \ln\left(\frac{k_b R + k_l}{k_b R_0 + k_l}\right) - k_b R + \frac{k_b}{2}R_0}.$$

Blow-up of $Y(R)$ occurs for $R = R^*$ for which the denominator is 0, i.e.

(S1.16)
$$k_l \ln\left(\frac{k_l R^* + k_b}{k_l R_0 + k_b}\right) - k_b R^* + \frac{k_b}{2}R_0 = 0.$$

5

Eq. S1.16 implies that $R(t_{gel}) = R^*$. To determine t_{gel}, we find the solution of Eq. S1.9 that satisfies the condition $R(0) = R_0$ and obtain

(S1.17)
$$t_{gel} = \frac{1}{k_l R^*} - \frac{1}{k_l R_0} - \frac{k_b}{2k_l^2} \ln\left(\frac{(k_b R^* + k_l)R_0}{(k_b R_0 + k_l)R^*}\right).$$

To find $M_{00}(t_{gel})$, we begin by solving Eq. S1.13 and imposing the condition $M_{00}(R_0) = \frac{R_0}{2}$ to obtain

(S1.18)
$$M_{00}(R) = \frac{2R}{3} - \frac{R_0}{6} - \frac{k_l}{3k_b} \ln\left(\frac{k_b R + k_l}{k_b R_0 + k_l}\right).$$

Since at gel time $R = R^*$, the last equation implies that

(S1.19)
$$M_{00}(t_{gel}) = \frac{2R^*}{3} - \frac{R_0}{6} - \frac{k_l}{3k_b} \ln\left(\frac{k_b R^* + k_l}{k_b R_0 + k_l}\right).$$

Using Eq. S1.16, this becomes

(S1.20)
$$M_{00}(t_{gel}) = \frac{R^*}{3} = \frac{R(t_{gel})}{3}.$$

6

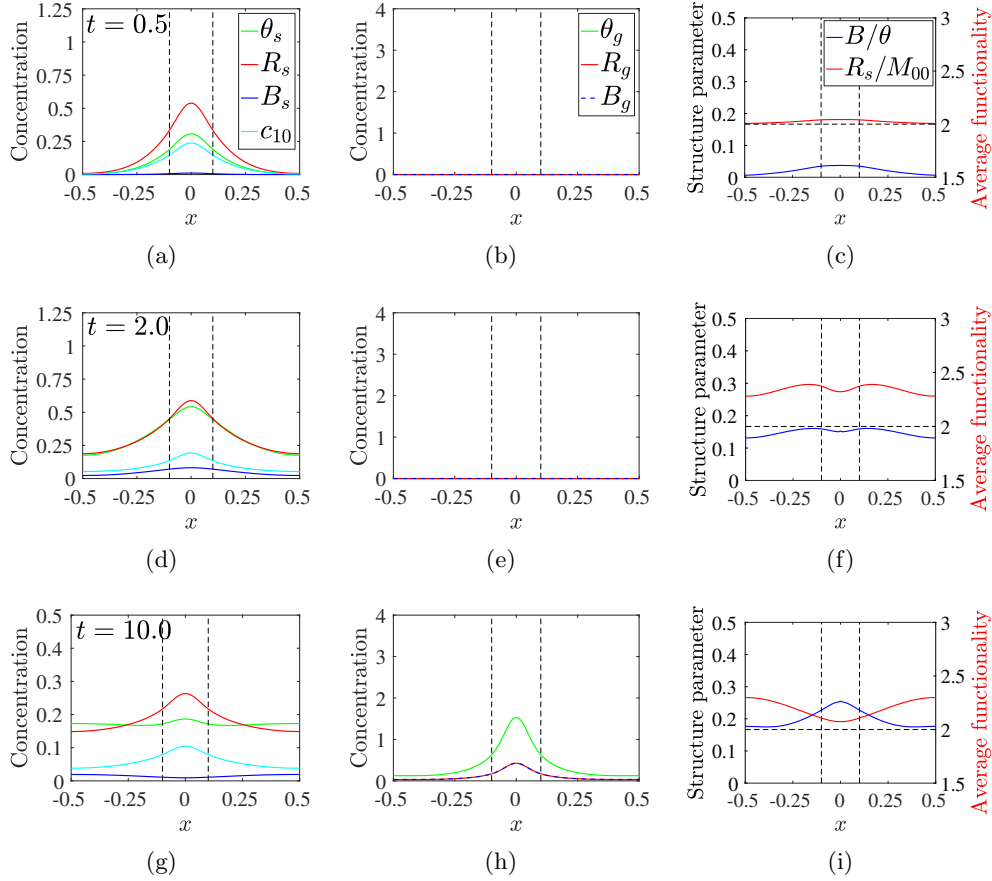## S1.8. Additional Results - Variations in Source Rate λ.

Fig. S2: PDE model simulations with source rate $S_{10}(x,t)$ given in Eq. 3.12 with $m_0 = 8$, $k_b = 4$, $D = 0.04$, $\boldsymbol{\lambda = 1/4}$. Snapshots of sol variables (left) gel variables (middle), and structure variables (right) at the times indicated for each row. Note change in vertical scale in left column. Black dashed vertical lines show extent of source's spatial support.
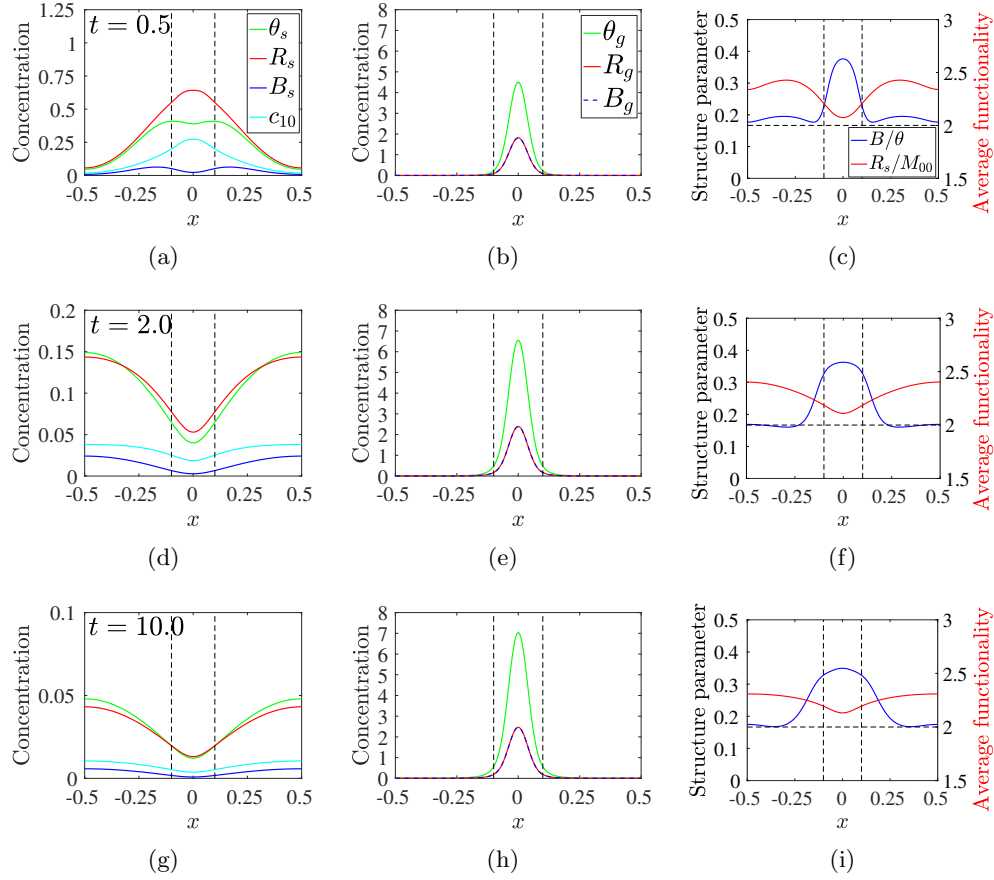
7

Fig. S3: PDE model simulations with source rate $S_{10}(x,t)$ given in Eq. 3.12 with $m_0 = 8$, $k_b = 4$, $D = 0.04$, $\boldsymbol{\lambda = 4.0}$. Snapshots of sol variables (left) gel variables (middle), and structure variables (right) at the times indicated for each row. Note change in vertical scale in left column. Black dashed vertical lines show extent of source's spatial support.

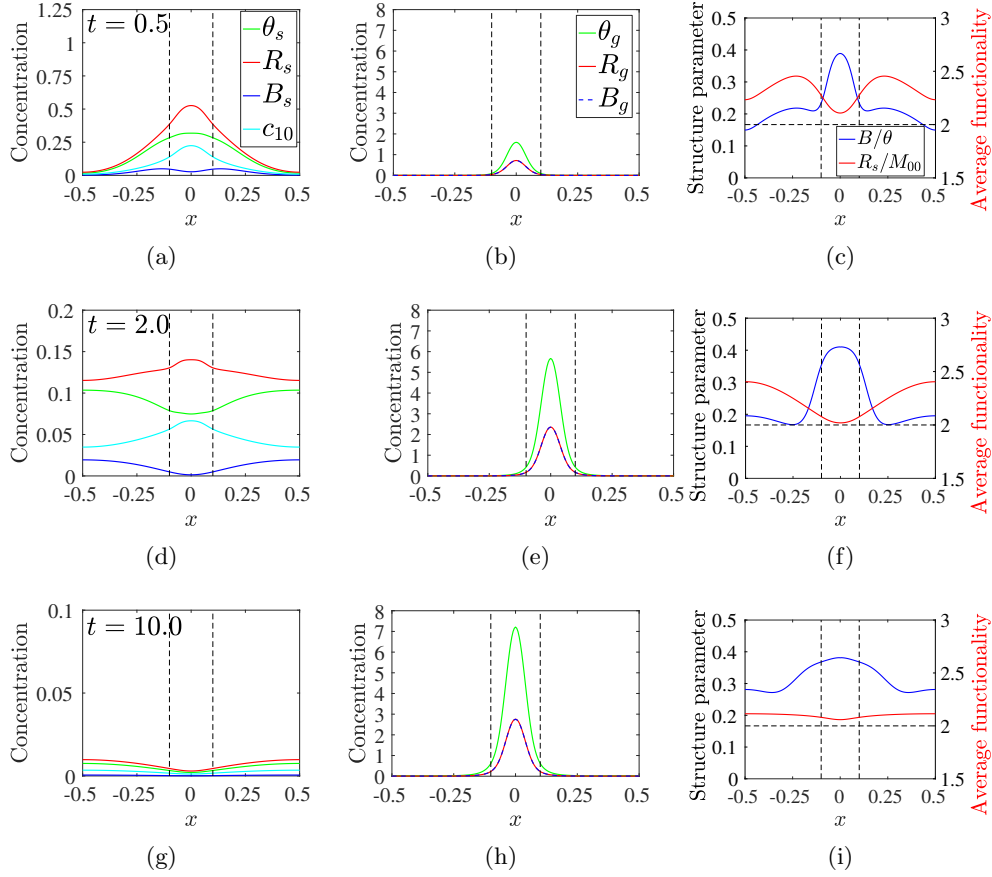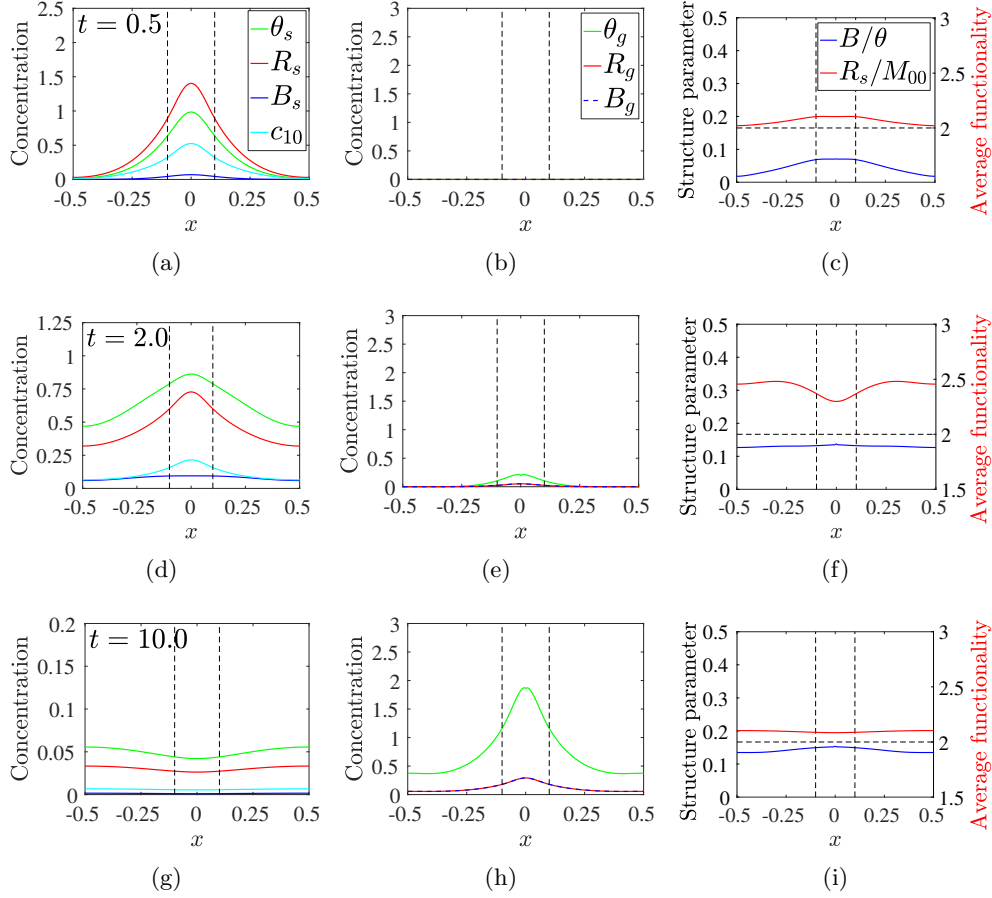**S1.9. <u>Additional Results - Variations in Branching Rate k_b.</u>**

Fig. S4: PDE model simulations with source rate $S_{10}(x,t)$ given in Eq. (3.12) with $m_0 = 8$, $\mathbf{k_b = 16}$, $\lambda = 1$, $D = 0.04$. Snapshots of sol variables (left) gel variables (middle), and structure variables (right) at the times indicated for each row. Note change in vertical scale in left column. Black dashed vertical lines show extent of source's spatial support.

9

Fig. S5: PDE model simulations with source rate $S_{10}(x,t)$ given in Eq. 3.12 with $m_0 = 8$, $\mathbf{k_b} = \mathbf{1}$, $\lambda = 1$, $D = 0.04$. Snapshots of sol variables (left) gel variables (middle), and structure variables (right) at the times indicated for each row. Note change in vertical scale in left column. Black dashed vertical lines show extent of source's spatial support.

10

S1.10. Additional Results - Variations in Diffusivity D and D_1.
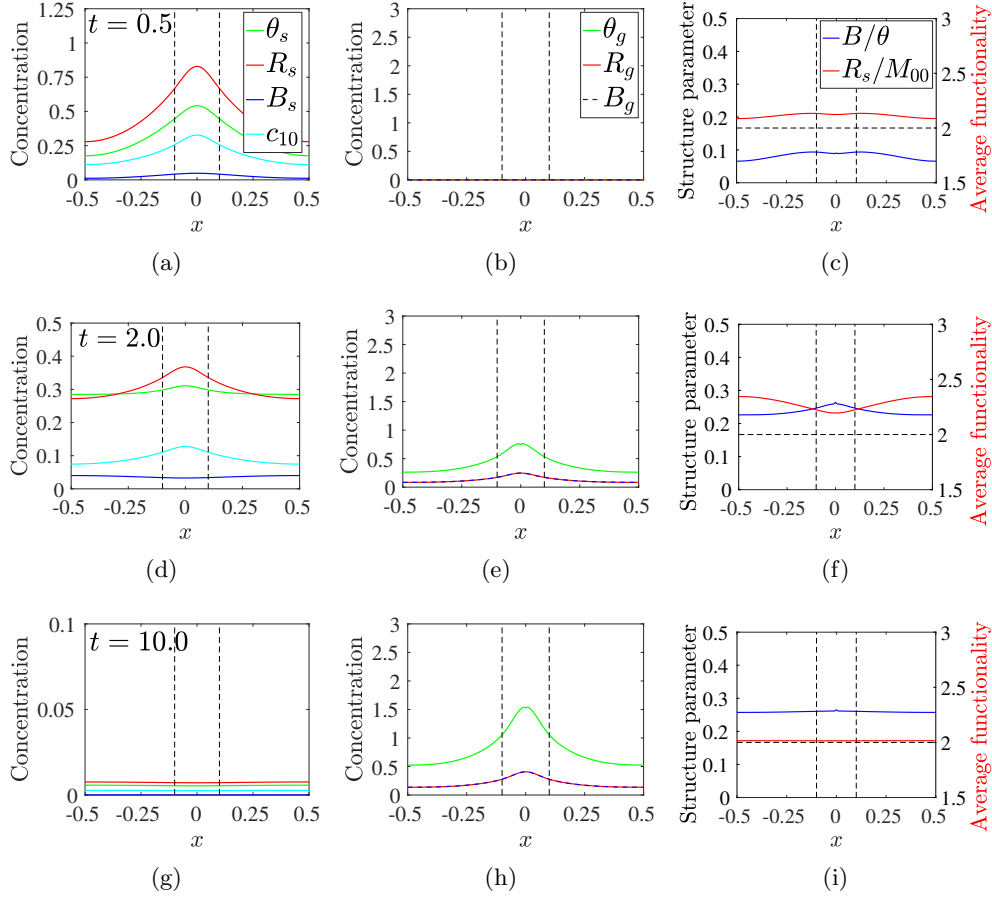
Fig. S6: PDE model simulations with source rate $S_{10}(x,t)$ given in Eq. (3.12) with $m_0 = 8$, $k_b = 4$, $\lambda = 1$, $\mathbf{D = 0.16}$. Snapshots of sol variables (left) gel variables (middle), and structure variables (right) at the times indicated for each row. Note change in vertical scale in left column. Black dashed vertical lines show extent of source's spatial support.
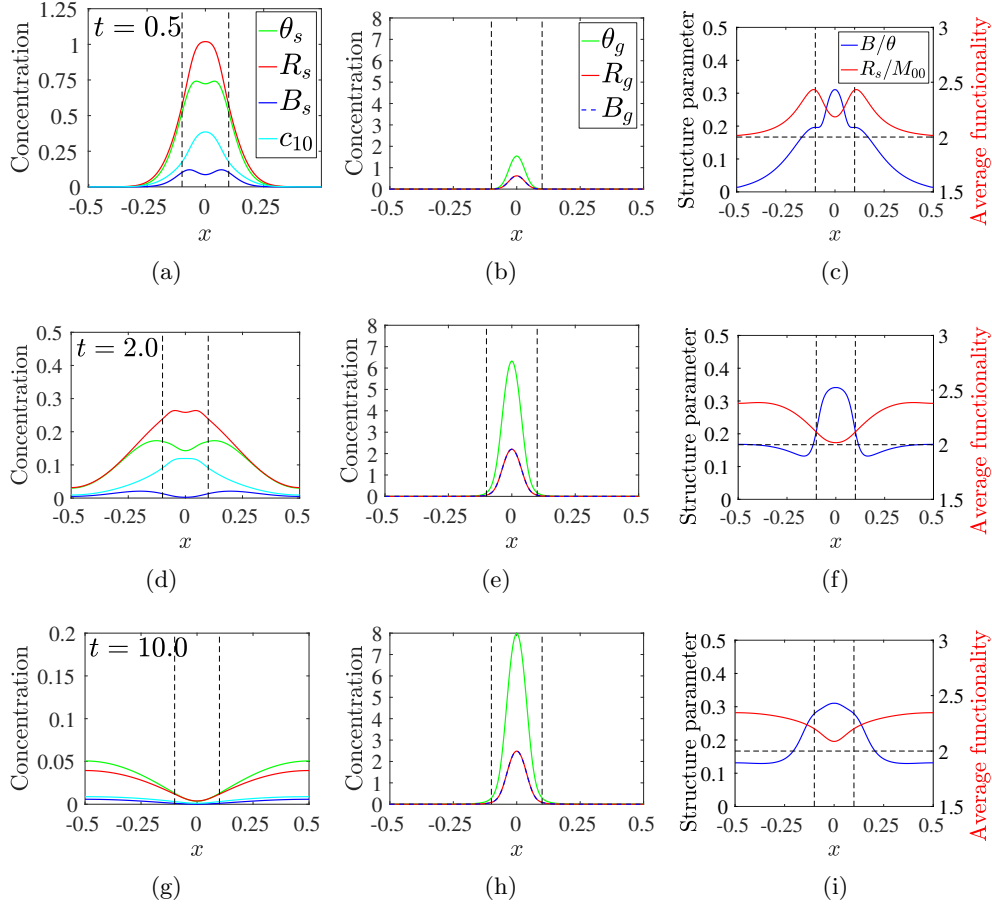
11

Fig. S7: PDE model simulations with source rate $S_{10}(x,t)$ given in Eq. 3.12 with $m_0 = 8$, $k_b = 4$, $\lambda = 1$, $\mathbf{D = 0.01}$. Snapshots of sol variables (left) gel variables (middle), and structure variables (right) at the times indicated for each row. Note change in vertical scale in left column. Black dashed vertical lines show extent of source's spatial support.
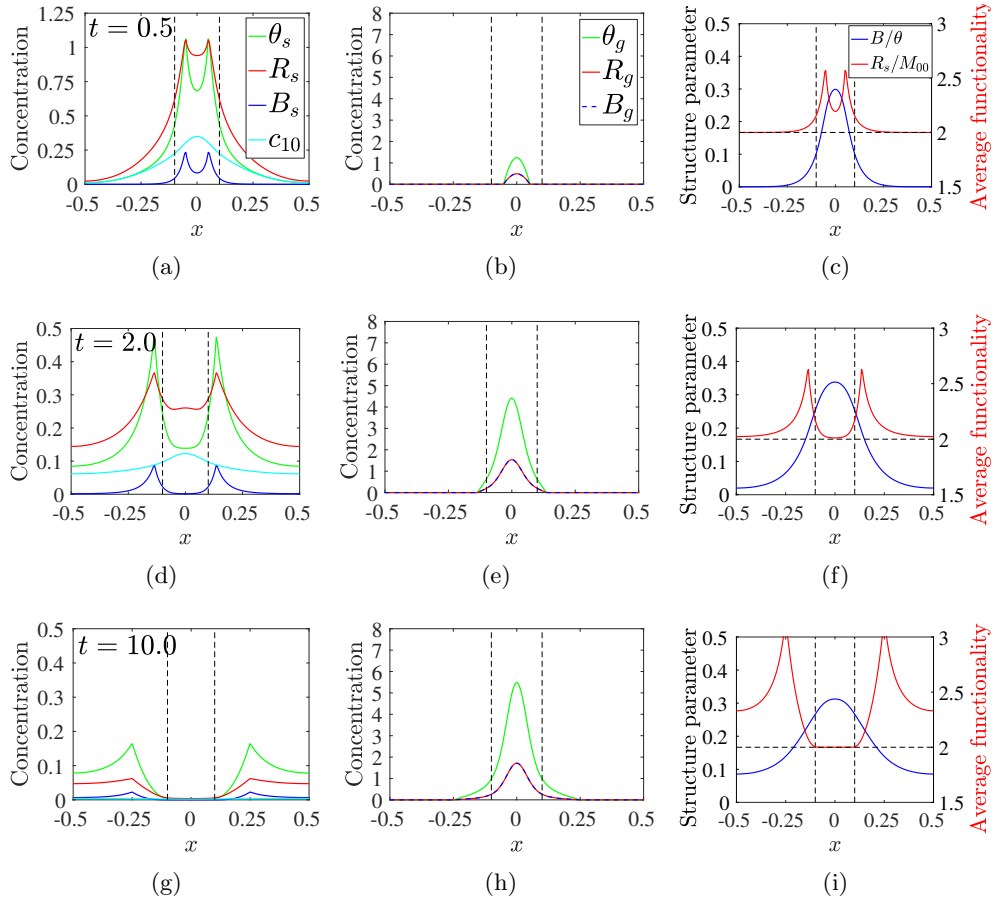
12

Fig. S8: PDE model simulations with source rate $S_{10}(x,t)$ given in Eq. 3.12 with $m_0 = 8$, $k_b = 4$, $\lambda = 1$, $\mathbf{D = 0}$, $\mathbf{D_1 = 0.04}$. Snapshots of sol variables (left) gel variables (middle), and structure variables (right) at the times indicated for each row. Note change in vertical scale in left column. Black dashed vertical lines show extent of source's spatial support.
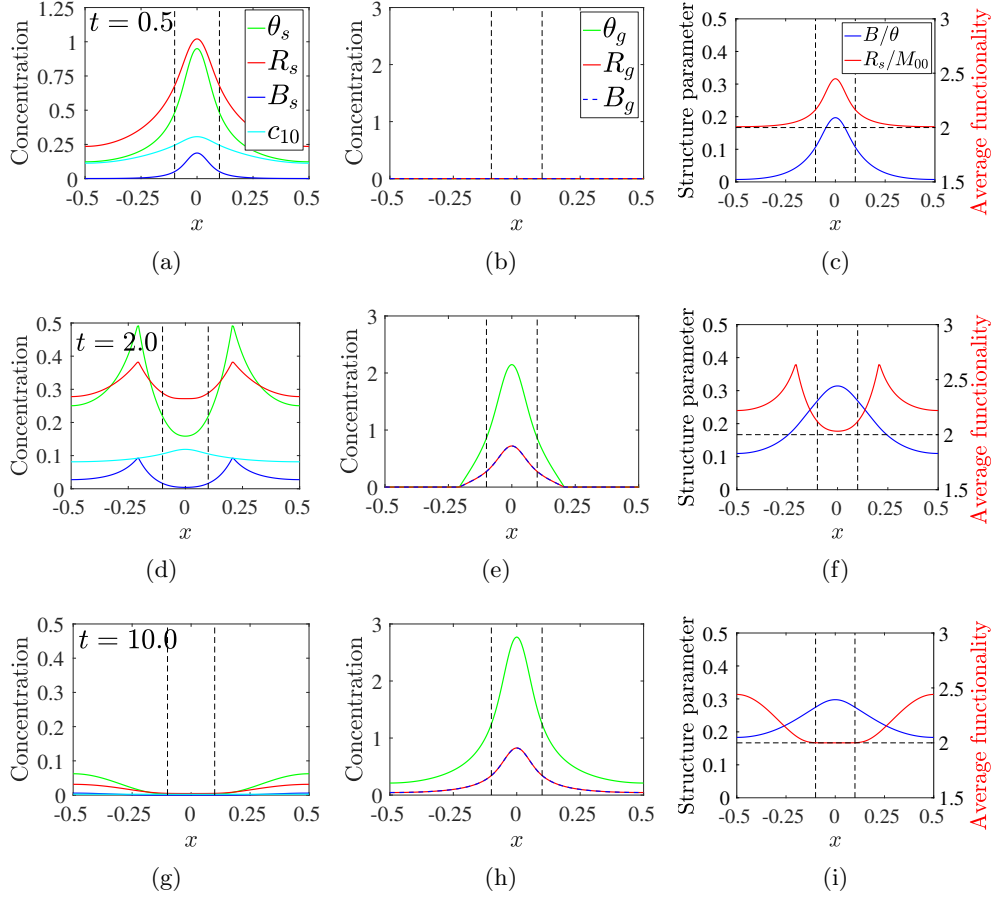
Fig. S9: PDE model simulations with source rate $S_{10}(x,t)$ given in Eq. 3.12 with $m_0 = 8$, $k_b = 4$, $\lambda = 1$, $\mathbf{D} = \mathbf{0}$, $\mathbf{D_1} = \mathbf{0.16}$. Snapshots of sol variables (left) gel variables (middle), and structure variables (right) at the times indicated for each row. Note change in vertical scale in left column. Black dashed vertical lines show extent of source's spatial support.